Catal Lett (2012) 142:452–459
DOI 10.1007/s10562-012-0789-1

Negative Effects of CO_2 in the Feed Stream on the Catalytic Performance of Precipitated Iron-Based Catalysts for Fischer–Tropsch Synthesis

Dong Hyun Chun · Ho-Tae Lee · Jung-Il Yang · Hak-Joo Kim · Jung Hoon Yang · Ji Chan Park · Byeong-Kwon Kim · Heon Jung

Received: 21 December 2011 / Accepted: 22 February 2012 / Published online: 17 March 2012

Abstract Fischer–Tropsch synthesis was carried out over precipitated iron-based catalysts with different amounts of CO_2 in the feed stream while maintaining both total reaction pressure (1.5 MPa) and partial pressure of $H_2 + CO$ (0.75 MPa) using an inert balance gas, N_2. The CO_2 in the feed stream decreased the rate of hydrocarbon formation, but it had no significant influence on the carbon number distribution of hydrocarbons. The CO_2 in the feed stream also suppressed CO_2 formation, decreasing both CO conversion and CO_2 selectivity. We attribute the decreased reaction rate to the partial competition in the adsorption behavior between CO and CO_2 as revealed in the temperature-programmed desorption.

Keywords Indirect coal liquefaction · Fischer–Tropsch synthesis · Precipitated iron-based catalysts · Effects of CO_2 · Adsorption of CO and CO_2

1 Introduction

Fischer–Tropsch synthesis (FTS) has received much attention as an essential part of the indirect coal liquefaction (ICL) process. In the ICL process, iron-based catalysts are highly promising for the FTS due to their potential activity for a water–gas shift (WGS) reaction as well as their high activity and low cost, as coal gasification produces a synthesis gas with a low H_2/CO ratio ($\leq$1.0) [1–4]. CO_2 generation inevitably accompanies the production of a synthesis gas via coal gasification, limiting the net efficiency of carbon utilization in the whole ICL process [2–4]. In general, the CO_2 has been separated from the feed stream, but it is potentially desirable to use the raw feed stream without an extra CO_2 separation process from the view point of heat/energy efficiency and facility simplification. Therefore, it is worth investigating the effects of CO_2 in the feed stream on the catalytic performance of industrial iron-based catalysts for the FTS in a synthesis gas with a low H_2/CO ratio ($\leq$1.0).

Several researchers have reported the FTS over iron-based catalysts in a CO_2-containing synthesis gas [5–13], but previous works on the FTS in a CO_2-containing synthesis gas with a low H_2/CO ratio ($\leq$1.0) are not abundant. Liu et al. [5] investigated the effects of co-feeding CO_2 on the Fe–Mn FTS catalysts in a synthesis gas with a low H_2/CO ratio (=1.0) by varying added CO_2 partial pressure in the feed stream at fixed total pressure and at fixed partial pressure of $H_2 + CO$, respectively. In other words, the partial pressure of $H_2 + CO$ decreases as the partial pressure of CO_2 increases at fixed total pressure, and the total pressure increases with increased CO_2 partial pressure at fixed partial pressure of $H_2 + CO$. In their work, they found that the added CO_2 partial pressure did not strongly influence the catalytic performance in terms of CO conversion and hydrocarbon selectivity during the FTS at 320 °C and fixed partial pressure of $H_2 + CO$. In contrast, at 260 °C and fixed total pressure, the CO conversion gradually decreased with the increased amount of CO_2 co-feeding, but

Electronic supplementary material The online version of this article (doi:10.1007/s10562-012-0789-1) contains supplementary material, which is available to authorized users.

D. H. Chun · H.-T. Lee · J.-I. Yang · H.-J. Kim · J. H. Yang · J. C. Park · B.-K. Kim · H. Jung (✉)
Clean Fuel Department, Korea Institute of Energy Research, 71-2 Jang-Dong, Yuseong-Gu, Daejeon 305-343, Republic of Korea
e-mail: jungh@kier.re.kr

D. H. Chun
e-mail: cdhsl@kier.re.kr

the hydrocarbon selectivity was not reported. Yates and Satterfield [6] also reported that the CO_2 is relatively inert during the FTS over fused magnetite catalysts in a synthesis gas with $H_2/CO = 0.67–0.72$ at fixed partial pressure of $H_2 + CO$. In the cases other than those by Liu et al. [5] and Yates and Scatterfield [6], most researchers either carried out the FTS in a synthesis gas with a high H_2/CO ratio ($\geq$2.0) which can simulate methane reforming or H_2-assisted biomass gasification, or they focused their attention on a comparison between the CO_2 hydrogenation and the FTS [7–11]. Furthermore, some conclusions are still controversial. It is generally accepted that the different conclusions result from the difference in the reaction condition/system and catalyst formulation.

In this study, we investigated the effects of CO_2 in the feed stream on the catalytic performance of industrially important Fe/Cu/K/SiO_2 catalysts in a low temperature FTS condition (<280 °C) with a low H_2/CO ratio (=1.0). Different amounts of CO_2 were added into the feed stream, carefully maintaining both total reaction pressure and partial pressure of $H_2 + CO$ using an inert balance gas, N_2, to exclude the potential effects of total pressure and $H_2 + CO$ partial pressure. We focused our particular attention on the effects of CO_2 on the catalytic activity and selectivity of the iron-based catalysts and the adsorption behavior of CO over the catalysts.

2 Experimental

The catalysts used in this study were prepared through a combination of a co-precipitation technique and a spray-drying method. In brief, a sodium carbonate solution was added to a solution containing both $Fe(NO_3)_3$ and $Cu(NO_3)_2$ in the desired ratio at 80 ± 1 °C until the pH reached 8.0 ± 0.1. The precipitate slurry was filtered, washed with distilled water, and subsequently re-slurried in distilled water. After completing the washing process, the required amount of K_2CO_3 solution and colloidal suspension of SiO_2 were added to the precipitate slurry, and the final mixture was spray-dried (inlet: 200 °C; outlet: 95 °C). Then, the spray-dried sample was calcined at 400 °C for 8 h. The chemical composition of the catalysts as analyzed by means of X-ray fluorescence spectroscopy (Rigaku model ZSX Primus II) was 100Fe/5.33Cu/5.23 K/17.4SiO_2 in part per weight. The Brunauer–Emmett–Teller (BET) surface area, the single point pore volume, and the average pore diameter were 120 m^2/g, 0.320 cm^3/g, and 10.7 nm, respectively. The calcined catalysts were pressed into pellets and then crushed and sieved to obtain 300–600 μm particles for a test in a fixed-bed reactor.

The FTS was carried out in a fixed-bed reactor composed of stainless steel (5 mm i.d. and 180 mm length). The catalysts (0.8 g) were diluted with glass beads (1.6 g; 425–600 μm) and then charged into the fixed-bed reactor. The catalysts were activated in situ with $H_2 + CO$ ($H_2/CO = 1.0$, 3.0 $NL/g_{(cat)}$·h) at 280 °C and ambient pressure for 20 h. After the activation treatment, the FTS was performed at 275 °C and 1.5 MPa using a synthesis gas ($H_2/CO = 1.0$) with different CO_2 content. The flow rate and partial pressure of $H_2 + CO$ was carefully maintained at 3.0 $NL/g_{(cat)}$·h and 50% of the total reaction pressure, respectively. The remainder was filled with N_2 and CO_2, and the ratio of CO_2 to N_2 was adjusted: $CO_2/N_2 = 0/100$, 24/76, 50/50, 100/0. The composition of the outlet gases was analyzed using an online gas chromatograph (GC; Agilent, 3000A Micro-GC) equipped with molecular sieve and Plot Q columns. The flow rates of the outlet gases were measured by means of a wet-gas flow meter. The composition of wax and liquid products was analyzed by means of an offline GC (Agilent, 6890N) with a simulated distillation method (ASTM D2887) [14].

The influence of CO_2 on the adsorption behavior of CO was analyzed by means of temperature-programmed desorption (TPD) using CO and/or CO_2 as adsorbents. In order to simulate the adsorption behavior at the pseudo-steady-state, the catalysts in the working condition were used for the TPD. The catalysts in the working condition were prepared by activating the fresh catalysts and subsequently exposing the activated catalysts to the reaction environment ($CO_2/N_2 = 0/100$) using the same process described above. After exposing the catalysts to the reaction environment for 114 h, the reactor was purged with N_2 (purity: 99.999%) for 6 h, cooled to the room temperature, and depressurized to 0.3 MPa. Then, the reactor was sealed and transferred to a glove box in a N_2 atmosphere (purity: 99.999%). After carefully withdrawing the catalysts from the reactor, the catalysts were washed with hexane to remove residual liquid/solid hydrocarbons from the catalysts. Then, the catalysts (about 200 mg) were loaded into the sample cell, and the sample cell was sealed and transferred to the equipment for the TPD. The catalysts were purged with a carrier gas, He, at 280 °C for 20 h to remove potential impurities remaining on the surface of the catalysts. After cooling the catalysts to 50 °C, CO or CO_2 was introduced into the sample cell for 30 min and this was followed by purging with the carrier gas for 30 min to remove weakly adsorbed species. The TPD was carried out up to 280 °C in the flow of carrier gas at a heating rate of 6 °C/min, and the temperature was then held at the maximum temperature for 40 min. The amount of desorbed gases was measured by means of a thermal conductivity detector (TCD). The amount of CO and CO_2 desorption was calculated separately by performing the TPD with and without using a CO_2 removal trap (Ascarite, 223921 Aldrich). For all measurements, we obtained at least two

TPD profiles to check the reproducibility of the results and confirmed that the TPD profiles showed reasonable reproducibility under all measurement conditions (see Supplementary Information for details).

3 Results and Discussions

The catalytic performance with different CO_2 content was evaluated at 275 °C. In addition to the unreacted CO and H_2, CH_4, C_2–C_4 hydrocarbons, and CO_2 were detected in the outlet gases. Liquid hydrocarbons and H_2O were obtained in the cold trap (1 °C), and solid hydrocarbons were also obtained in the hot trap (240 °C). The amount of effluent CO_2 in the outlet gases was larger than the amount of CO_2 added in the feed stream for all reaction conditions, indicating that the formation of hydrocarbons via the FTS (Eqs. 1, 2) proceeds accompanying the formation of CO_2 via WGS (Eq. 3), as follows:

$$n\mathrm{CO} + (2n+1)\mathrm{H_2} \leftrightarrow \mathrm{C}_n\mathrm{H}_{2n+2} + n\mathrm{H_2O}\ (n \geq 1), \quad (1)$$

$$n\mathrm{CO} + 2n\mathrm{H_2} \leftrightarrow \mathrm{C}_n\mathrm{H}_{2n} + n\mathrm{H_2O}\ (n \geq 2), \quad (2)$$

$$\mathrm{CO} + \mathrm{H_2O} \leftrightarrow \mathrm{CO_2} + \mathrm{H_2}. \quad (3)$$

The CO conversion gradually decreased with increased time and then reached a pseudo-steady-state after about 90 h of reaction (see supplementary information for details). Therefore, we assumed that the catalytic performance during 90–204 h of reaction is representative of the performance of the catalysts used in this study.

Figure 1 shows the overall CO conversion and the overall H_2 conversion during 90–204 h of reaction as a function of inlet CO_2 content. In this graph, 0% of inlet CO_2 content means that 50% of total inlet gases were filled with N_2. As the inlet CO_2 content increased, the N_2 was replaced with the equivalent amount of CO_2, maintaining the total reaction pressure at 1.5 MPa and the partial pressure of H_2 + CO at 0.75 MPa, respectively. The CO conversion and the H_2 conversion showed obviously different trends with increased inlet CO_2 content. While the CO conversion gradually decreased as the inlet CO_2 content increased, the H_2 conversion showed no considerable difference with increased inlet CO_2 content. The total CO conversion can be divided into the CO conversion to hydrocarbons (CO to HC) and the CO conversion to CO_2 (CO to CO_2) as shown in Fig. 1. The CO to HC and the CO to CO_2 reflect the rate of hydrocarbon formation and the rate of CO_2 formation, respectively. Both the CO to HC and the CO to CO_2 decreased with increased inlet CO_2 content, which implies that the CO_2 in the feed stream has a negative effect both on the formation of hydrocarbons via the FTS and on the formation of CO_2 via WGS. The CO to CO_2 showed a more pronounced decline with increased

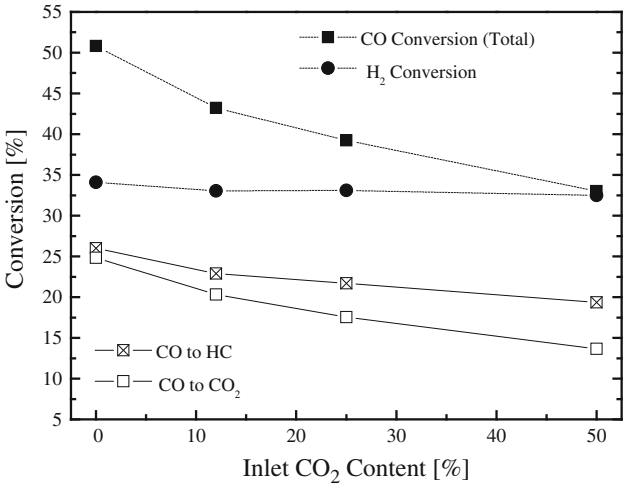

Fig. 1 The overall CO conversion and the overall H_2 conversion during 90–204 h of reaction in the Fischer–Tropsch synthesis as a function of inlet CO_2 content. In the case of CO conversion, the CO conversion to hydrocarbons (CO to HC) and the CO conversion to CO_2 (CO to CO_2), which respectively reflect the rate of hydrocarbon formation and the rate of CO_2 formation, are inserted in addition to the total CO conversion

inlet CO_2 content than the CO to HC, indicating that the CO_2 formation is more strongly affected by the CO_2 in the feed stream compared to the hydrocarbon formation.

The overall CO_2 selectivity and the overall oxygen to H_2O selectivity during the 90–204 h of reaction are given in Fig. 2a as a function of inlet CO_2 content. The oxygen to H_2O selectivity is defined as the fraction of the oxygen in the converted CO that appears as H_2O. The CO_2 selectivity monotonously decreased as the CO_2 content in the feed stream increased, and the oxygen to H_2O selectivity showed the opposite trend to the CO_2 selectivity. The decreased CO_2 selectivity and the increased oxygen to H_2O selectivity are potentially attributed to the suppression of CO_2 formation via WGS (Eq. 3) or the promotion of reverse WGS (reverse of Eq. 3) as these reactions approach the equilibrium state with increased inlet CO_2 content. The approach to the equilibrium state in the WGS reaction can be estimated by a parameter, η_i, as follows:

$$\eta_i = \frac{1}{K_p}\frac{P_{CO_2} P_{H_2}}{P_{CO} P_{H_2O}}, \quad (4)$$

where K_p and P_j are the equilibrium constant for WGS and the partial pressure of reaction species j, respectively. As the WGS reaction approaches the equilibrium state, the value of η_i increases from 0 to 1. As shown in Fig. 2b, the η_i showed higher value at the higher inlet CO_2 content, indicating that the WGS reaction approaches the equilibrium state as the inlet CO_2 content increased. But, considering that the η_i was much lower than the equilibrium value, 1.0, at all reaction conditions, the occurrence of WGS is supposed to be far from

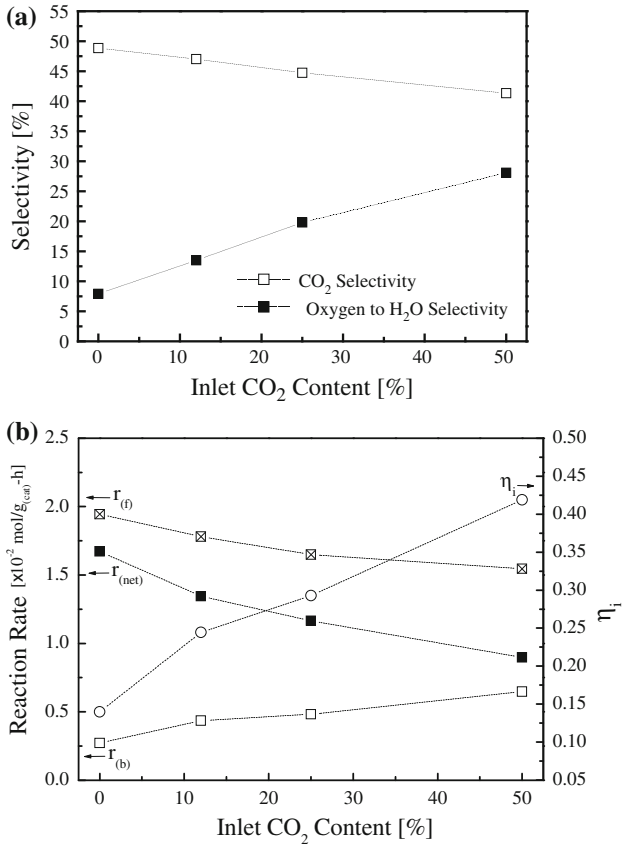

Fig. 2 **a** The overall CO_2 selectivity and the overall oxygen to H_2O selectivity during 90–204 h of reaction in the Fischer–Tropsch synthesis as a function of inlet CO_2 content. **b** The equilibrium parameter for the WGS reaction (η_i), the net rate of CO_2 formation ($r_{(net)}$), forward rate of WGS ($r_{(f)}$), and the reverse rate of WGS ($r_{(b)}$) during 90–204 h of reaction in the Fischer–Tropsch synthesis as a function of inlet CO_2 content

the equilibrium state under the FTS conditions. This corresponded well with the previous works by Krishnamoorthy et al. [7] and Pour et al. [15]. The approach to the equilibrium state can kinetically influence the WGS reaction. According to the previous studies [7, 15, 16], the net rate of CO_2 formation via WGS can be expressed as a function of the forward rate of WGS and the equilibrium parameter, η_i, as follows:

$$r_{(net)} = r_{(f)} - r_{(b)} = r_{(f)}\left(1 - \frac{1}{K_p}\frac{P_{CO_2} P_{H_2}}{P_{CO} P_{H_2O}}\right) = r_{(f)}(1 - \eta_i), \quad (5)$$

where $r_{(net)}$ is the net rate of CO_2 formation, $r_{(f)}$ is the forward rate of WGS, and $r_{(b)}$ is the reverse rate of WGS. Thus, the forward rate of WGS can be calculated from the net rate of CO_2 formation divided by $(1-\eta_i)$. The net rate of CO_2 formation, the forward rate of WGS, and the reverse rate of WGS are also presented in Fig. 2b. The net rate of CO_2 formation monotonously decreased with increased inlet CO_2 content, which well corresponds to the decreased CO to CO_2 in Fig. 1. The forward rate of WGS also decreased with increased inlet CO_2 content, but it decreased less steeply than the net rate of CO_2 formation, which means that the approach to the equilibrium state promotes the conversion of CO_2 to CO via the reverse WGS reaction (reverse of Eq. 3). Consequently, the decreased rate of forward WGS and the increased rate of reverse WGS may contribute to the decreased CO_2 selectivity, the increased oxygen to H_2O selectivity (Fig. 2a), and no significant difference in the H_2 conversion (Fig. 1).

The effects of CO_2 on the hydrocarbon distribution are shown in Fig. 3. As shown in Fig. 3a, the selectivity of paraffinic hydrocarbons in gaseous phase (C_1–C_4) showed a decreasing trend as the inlet CO_2 content increased, but that of 1-olefins in C_2–C_4 hydrocarbons increased with increased inlet CO_2 content. The increased fraction of 1-olefins in gaseous hydrocarbons is potentially attributed

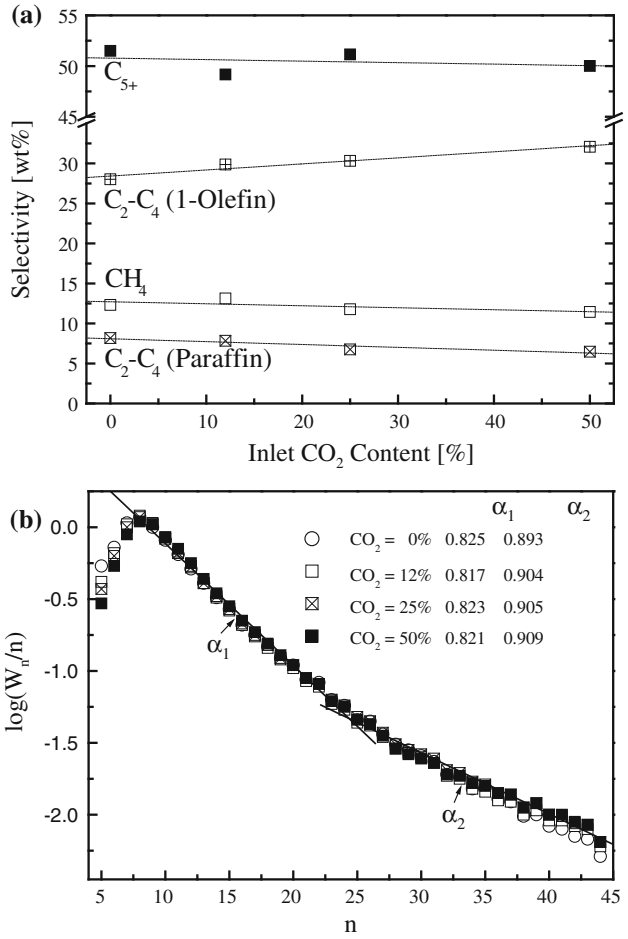

Fig. 3 **a** The hydrocarbon distribution during 90–204 h of reaction in the Fischer–Tropsch synthesis as a function of inlet CO_2 content: CH_4 and C_2–C_4 (1-olefin), C_2–C_4 (Paraffin), and C_{5+} hydrocarbons. **b** The Anderson–Schulz–Flory distribution of liquid hydrocarbons and the chain growth probability (α_1 from C_8 to C_{24} and α_2 from C_{24} and C_{44}) per each inlet CO_2 content during 90–204 h of reaction in the Fischer–Tropsch synthesis

to the decreased H_2/CO ratio with increased inlet CO_2 content. As described above, the decreased rate of forward WGS and the increased rate of reverse WGS with increased inlet CO_2 content can keep the reaction environment with a lower H_2/CO ratio, possibly suppressing the secondary hydrogenation of hydrocarbon chains to form paraffinic hydrocarbons. The overall selectivity of C_{5+} hydrocarbons showed an even trend with increased CO_2 content as the increased selectivity of 1-olefins in C_2–C_4 hydrocarbons offsets the decreased selectivity of paraffinic hydrocarbons in gaseous phase (C_1–C_4). Therefore, it is suggested that the presence of CO_2 in the feed stream does not significantly influence the chain growth of hydrocarbons during FTS. The Anderson–Schulz–Flory (ASF) distribution of the liquid products is also presented in Fig. 3b. The ASF distribution is expressed by the following equation (Eq. 6) [4, 17]:

$$\log(W_n/n) = \log\alpha \cdot n + \log(\ln^2\alpha), \quad (6)$$

where W_n is the weight fraction of hydrocarbons with carbon number n, and α is the chain growth probability of the hydrocarbons. Using this equation, the chain growth probability, α, can be directly derived by calculating the slope of the graph; a gentler slope indicates a higher value of α. The ASF distribution for each reaction condition can be well fitted by two linear regressions; in other words two values of α (α_1 from C_8 to C_{24} and α_2 from C_{24} and C_{44}) can be derived from the graph. An ASF distribution with these two α types has been reported as typical behavior of iron-based catalysts promoted by potassium, as the potassium is not homogenously distributed on the catalyst surface. Potassium-lean sites possibly generate a low α value (α_1), and potassium-rich sites generate a high α value (α_2) [17, 18]. As given in Fig. 3b, the ASF distribution of the liquid products showed almost the same α values (α_1 and α_2) under all reaction conditions, which confirms the negligible effects of CO_2 on the chain growth of hydrocarbons during the FTS. This is strongly supported by the previous works by Davis and co-workers [12, 13] which suggest that different surface chemical species are involved for chain initiation and for chain propagation. The CO_2 in the feed stream is supposed to be involved with chain initiation decreasing the rate of hydrocarbon formation (Fig. 1), but it may not be involved with chain propagation without influencing the carbon number distribution of hydrocarbons (Fig. 3).

The effects of CO_2 in the feed stream on catalytic performance can be closely related to its effects on the adsorption behavior of CO over the catalysts. TPD is often used as an effective tool to investigate the adsorption behavior of reactant gases in the FTS [19–21]. Figure 4 shows the TPD profiles of different adsorption species with and without using a CO_2 removal trap: single adsorption of

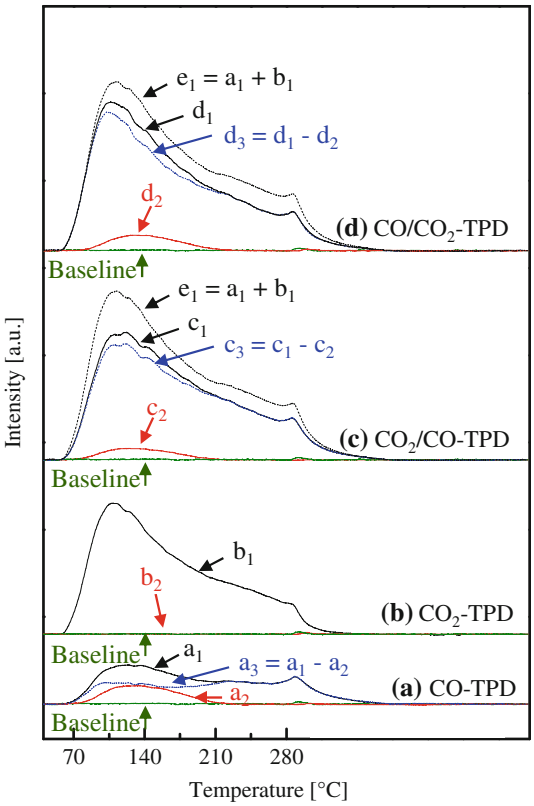

Fig. 4 The TPD profiles of different adsorption species: single adsorption of (a_1, a_2) CO and (b_1, b_2) CO_2 and sequential adsorption of (c_1, c_2) CO_2 → CO and (d_1, d_2) CO → CO_2 (a_2, b_2, c_2, d_2) with and (a_1, b_1, c_1, d_1) without using a CO_2 removal trap

(a) CO and (b) CO_2 and sequential adsorption of (c) CO_2 → CO and (d) CO → CO_2. The noteworthy detail is as follows:

(i) Most of the strongly adsorbed CO desorbed as CO_2 during the desorption process when CO was used as an adsorbent (CO-TPD, CO_2/CO-TPD, and CO/CO_2-TPD). The TPD profiles without a CO_2 removal trap (Fig. 4a_1, c_1, d_1) showed two groups of desorption peaks: one at the low temperature corresponding to the desorption of weakly adsorbed species and the other at the high temperature corresponding to that of strongly adsorbed species [19–21]. Interestingly, the TPD profiles with a CO_2 removal trap (Fig. 4a_2, c_2, d_2) showed a major desorption peak only at low temperature, indicating that most of the strongly adsorbed CO desorbed as CO_2 at high temperature, possibly carrying the lattice oxygen, or via dissociation of CO. In contrast, when only CO_2 was used as an adsorbent, the TPD profiles with a CO_2 removal trap (Fig. 4b_2) were almost identical to the baseline, implying that the CO_2 desorbed as it was adsorbed, probably because the CO_2 is too stable to be converted to CO in the TPD condition.

Table 1 Quantitative analyses of CO and CO_2 desorption in the TPD profiles of different adsorption species

	Adsorption gas	Amount of desorption (μmol/g)		
		as CO	as CO_2	Total
CO-TPD	CO	a_2 4.09	a_3 11.0	15.1
CO_2-TPD	CO_2	–	b_1 35.9	35.9
CO_2/CO-TPD	$CO_2 \rightarrow CO$	c_2 2.50	c_3 36.9	39.4
CO/CO_2-TPD	$CO \rightarrow CO_2$	d_2 3.28	d_3 38.4	41.7

(ii) There was partial competition in the adsorption behavior between CO and CO_2. Both CO_2/CO-TPD and CO/CO_2-TPD profiles without a CO_2 removal trap (Fig. 4c_1, d_1) showed larger peaks than the CO-TPD (Fig. 4a_1) and the CO_2-TPD (Fig. 4b_1), but it was smaller than the summation of CO-TPD and CO_2-TPD (Fig. 4e_1). The amount of CO and CO_2 desorption is summarized in Table 1. In the case of CO-TPD, CO_2/CO-TPD, and CO/CO_2-TPD, the desorption profiles of CO_2 (Fig. 4a_3, c_3, d_3) were obtained by subtracting the desorption profiles with a CO_2 removal trap (Fig. 4a_2, c_2, d_2) from those without a CO_2 removal trap (Fig. 4a_1, c_1, d_1). The amount of CO and CO_2 desorption in the CO_2/CO-TPD (CO: 2.50 μmol/g, CO_2: 36.9 μmol/g) and that in the CO/CO_2-TPD (CO: 3.28 μmol/g, CO_2: 38.4 μmol/g) was smaller than the summation of that in the CO-TPD and CO_2-TPD (CO: 4.09 μmol/g, CO_2: $11.0 + 35.9 = 46.9$ μmol/g), which means that there is partial competition in the adsorption behavior between CO and CO_2.

The partial competition in the adsorption behavior between CO and CO_2 suggests that the CO and CO_2 are mainly adsorbed on the different sites, respectively. According to the previous study by Amenomiya and Pleizier [19], the CO_2 molecules are mainly adsorbed on the alkali surface but most of the CO molecules are adsorbed on the iron metal surface. Also, the partial competition between the adsorption of CO and CO_2 suggests that a certain fraction of iron surface, which mainly adsorbs the CO as active sites, is occupied by the CO_2. This is strongly supported by the previous study Dry et al. [22] which suggests that the CO_2 molecules are mainly adsorbed on the alkali promoter surface but in part adsorbed on the metallic iron. Consequently, the CO_2 in the feed stream suppresses both the hydrocarbon formation via the FTS and the CO_2 formation via forward WGS. Figure 5 shows the comparison of the hydrocarbon formation rate with the forward rate of WGS during 90–204 h of reaction as a function of inlet CO_2 content. The rate of hydrocarbon formation and the forward rate of WGS declined with increased inlet CO_2 content, displaying slopes almost

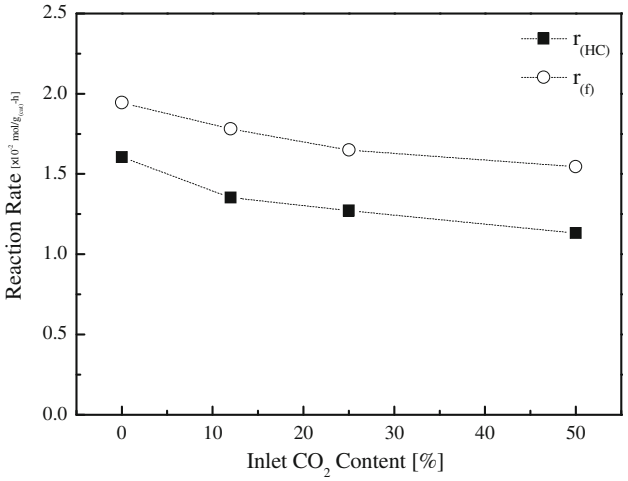

Fig. 5 The comparison of the hydrocarbon formation rate ($r_{(HC)}$) with the forward rate of WGS ($r_{(f)}$) during 90–204 h of reaction in the Fischer–Tropsch synthesis as a function of inlet CO_2 content

identical with each other. Therefore, it is suggested that the CO_2 in the feed stream almost equally suppresses the hydrocarbon formation via the FTS and the CO_2 formation via forward WGS. In other words, the number of CO_2 molecules which occupy the CO adsorption sites for the FTS may be almost equal to that of CO_2 molecules which occupy the CO adsorption sites for WGS. But, as the CO_2 in the feed stream promotes the consumption of CO_2 via reverse WGS (Fig. 2b), the overall rate of CO_2 formation (CO to CO_2) declined more pronouncedly with increased inlet CO_2 content than the overall rate of hydrocarbon formation (CO to HC) as shown in Fig. 1.

The effects of CO_2 in the feed stream on the catalytic performance of iron-based catalysts for the FTS can be summarized by Scheme 1, which is based on the experimental results obtained in this study. In Scheme 1, we presumed that the overall reaction at the steady state can be divided into three steps: the FTS step, the forward WGS step, and the reverse WGS step. The influence of CO_2 in the feed stream on the catalytic performance can be simply expressed as three variables, η_i, $k_{FT,i}$, and $k_{FW,i}$, which obviously have positive dependence on the inlet CO_2 content, and two constants, $r_{FT,0}$ and $r_{FW,0}$, as follows:

$$\text{CO conversion} = \{(r_{FT,0} - k_{FT,i}) + (1 - \eta_i)(r_{FW,0} - k_{FW,i})\}\ \%\ , \quad (7)$$

$$\text{CO to HC} = (r_{FT,0} - k_{FT,i})\%\ , \quad (7-1)$$

$$\text{CO to } CO_2 = (1 - \eta_i)(r_{FW,0} - k_{FW,i})\ \%\ , \quad (7-2)$$

$$CO_2 \text{ selectivity} = \frac{(1 - \eta_i)(r_{FW,0} - k_{FW,i})}{(r_{FT,0} - k_{FT,i}) + (1 - \eta_i)(r_{FW,0} - k_{FW,i})}, \quad (8)$$

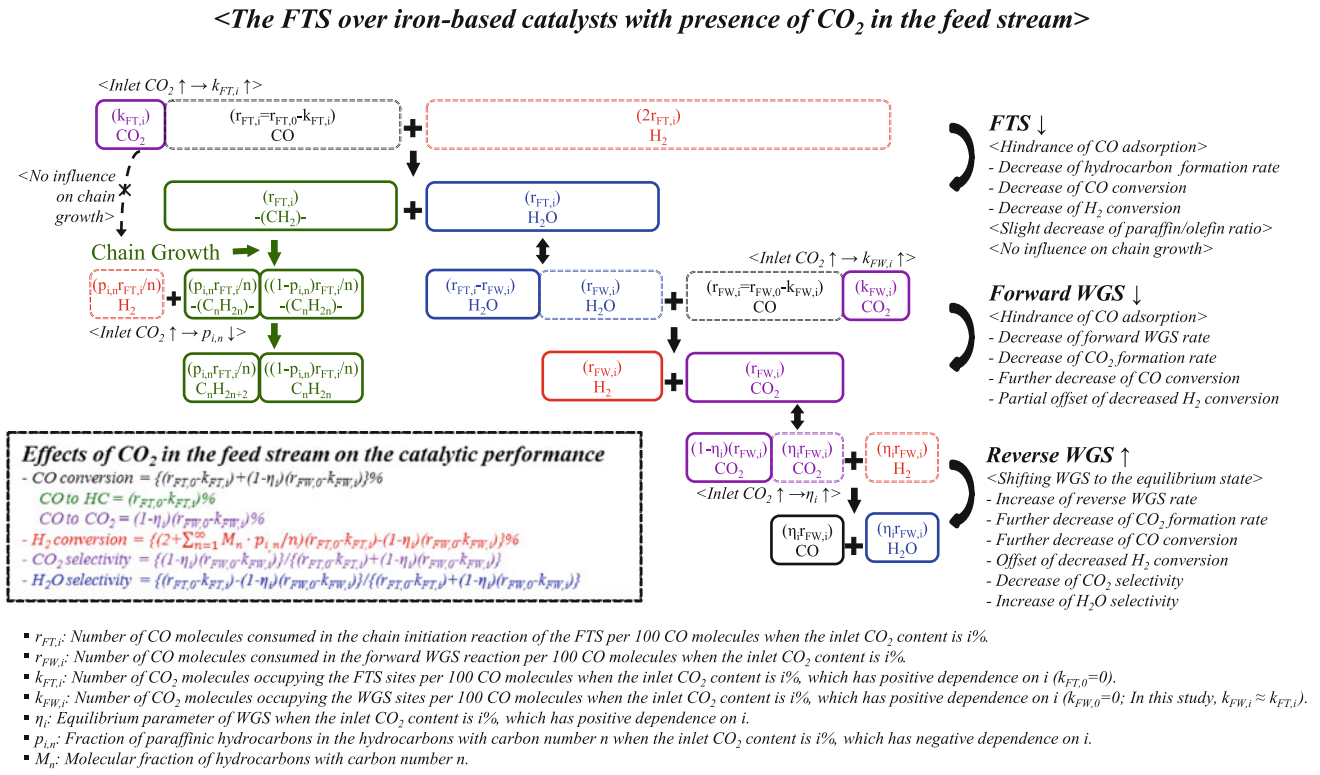

- $r_{FT,i}$: Number of CO molecules consumed in the chain initiation reaction of the FTS per 100 CO molecules when the inlet CO_2 content is i%.
- $r_{FW,i}$: Number of CO molecules consumed in the forward WGS reaction per 100 CO molecules when the inlet CO_2 content is i%.
- $k_{FT,i}$: Number of CO_2 molecules occupying the FTS sites per 100 CO molecules when the inlet CO_2 content is i%, which has positive dependence on i ($k_{FT,0}$=0).
- $k_{FW,i}$: Number of CO_2 molecules occupying the WGS sites per 100 CO molecules when the inlet CO_2 content is i%, which has positive dependence on i ($k_{FW,0}$=0; In this study, $k_{FW,i} \approx k_{FT,i}$).
- η_i: Equilibrium parameter of WGS when the inlet CO_2 content is i%, which has positive dependence on i.
- $p_{i,n}$: Fraction of paraffinic hydrocarbons in the hydrocarbons with carbon number n when the inlet CO_2 content is i%, which has negative dependence on i.
- M_n: Molecular fraction of hydrocarbons with carbon number n.

Scheme 1 Schematic summary: The effects of CO_2 in the feed stream on the catalytic performance of iron-based catalysts for the FTS

$$\text{Oxygen to } H_2O \text{ selectivity} = \frac{(r_{FT,0}-k_{FT,i})-(1-\eta_i)(r_{FW,0}-k_{FW,i})}{(r_{FT,0}-k_{FT,i})+(1-\eta_i)(r_{FW,0}-k_{FW,i})}, \quad (9)$$

where $r_{FT,0}$ and $r_{FW,0}$ are the number of CO molecules consumed in the FTS and forward WGS, respectively, per 100 CO molecules with the absence of CO_2 in the feed stream, and $k_{FT,i}$ and $k_{FW,i}$ are the number of CO_2 molecules occupying the FTS sites and the WGS sites, respectively, per 100 CO molecules when the inlet CO_2 content is i%. In case of the H_2 conversion, it needs another variable, $p_{i,n}$, which has negative dependence on the inlet CO_2 content, as follows:

$$H_2 \text{ conversion} = \left\{\left(2+\sum_{n=1} M_n \frac{p_{i,n}}{n}\right)(r_{FT,0}-k_{FT,i}) - (1-\eta_i)(r_{FW,0}-k_{FW,i})\right\}\%, \quad (10)$$

where $p_{i,n}$ is the fraction of paraffinic hydrocarbons in the hydrocarbons with carbon number n when the inlet CO_2 content is i%, and M_n is the molecular fraction of hydrocarbons with carbon number n. At the FTS step, the number of CO molecules adsorbed on the FTS sites decreases as a certain fraction of FTS sites is occupied by the CO_2 molecules, resulting in the decreased hydrocarbon formation rate (Fig. 5). Correspondingly, the CO conversion and the H_2 conversion decrease. In the case of H_2 conversion, it suffers another slight decrease due to the decreased fraction of paraffinic hydrocarbons with increased inlet CO_2 content. However, once the hydrocarbon chains are initiated, their growth is not supposed to be influenced by the CO_2 molecules (Fig. 3), probably because different surface chemical species are involved for chain initiation and for chain propagation as Davis and co-workers [12, 13] suggested. At the forward WGS step, the CO_2 molecules also occupy the CO adsorption sites for forward WGS, and, as a result the rate of forward WGS decreases, accompanying the further decrease of CO conversion and the partial offset of decreased H_2 conversion. At the reverse WGS step, the CO_2 molecules are much more favorably consumed to produce CO and H_2O as the WGS reaction approaches the equilibrium state due to the CO_2 in the feed stream. As a result, the CO conversion and the CO_2 formation rate decreases further and further (Fig. 1). Also, this step slightly decreases the CO_2 selectivity and significantly increases the oxygen to H_2O selectivity as shown in Fig. 2. But, in the case of H_2 conversion, it is not significantly affected by the CO_2 in the feed stream as the increased rate of reverse WGS offsets the decreased H_2 conversion.

4 Conclusion

The presence of CO_2 in the feed stream negatively influences the catalytic performance of iron-based FTS catalysts

and the adsorption behavior of CO over the catalysts. Our main results are summarized as follows:

1. The CO_2 in the feed stream lowered both the rate of hydrocarbon formation and the rate of CO_2 formation. In comparison with the rate of hydrocarbon formation, the rate of CO_2 formation showed a more pronounced decline with increased inlet CO_2 content, possibly due to the additional influence induced by the occurrence of reverse WGS.
2. While the CO_2 in the feed stream slightly increased the fraction of 1-olefins in C_2–C_4 hydrocarbons, it did not significantly influence the carbon number distribution of hydrocarbons in both gaseous phase and liquid phase.
3. The temperature-programmed desorption showed partial competition in the adsorption behavior between CO and CO_2, possibly contributing to the suppression in the hydrocarbon formation via the FTS and the CO_2 formation via forward WGS.

Acknowledgments This work was supported by the Major R&D Projects Program of the Korea Institute of Energy Research (KIER-GP2009-0013). The authors highly appreciate Mr. Geun-Bae Rhim (Hanbat National University, Republic of Korea) for his technical support in the experimental procedure.

References

1. Anderson RB (1984) The Fischer–Tropsch synthesis. Academic Press, Inc., New York
2. Dry ME (1990) Catal Today 6:183
3. Dry ME (2003) In: Horvárth IT (ed) Encyclopedia of catalysis, vol 3. Wiley-Interscience, New Jersey, pp 347–403
4. Steynberg AP, Dry ME (2004) Fischer–Tropsch technology. Elsevier, Amsterdam
5. Liu Y, Zhang C, Wang Y, Li Y, Hao X, Bai L, Xiang H, Xu Y, Zhong B, Li Y (2008) Fuel Process Technol 89:234
6. Yates IC, Satterfield CN (1989) Ind Eng Chem Res 28:9
7. Krishnamoorthy S, Li A, Iglesia E (2002) Catal Lett 80:77
8. Ning W, Koizumi N, Yamada M (2009) Energy Fuel 23:4696
9. Riedel T, Schulz H, Schaub G, Jun KW, Hwang JS, Lee KW (2003) Top Catal 26:41
10. Prasad PSS, Bae JW, Jun KW, Lee KW (2008) Catal Surv Asia 12:170
11. Gnanamani MK, Shafer WD, Sparks DE, Davis BH (2011) Catal Commun 12:936
12. Xu L, Bao S, Houpt DJ, Lambert SH, Davis BH (1997) Catal Today 36:347
13. Davis BH (2009) Catal Today 141:25
14. ASTM D2887-08 (1989) ASTM International, West Conshohocken
15. Pour AN, Shahri SMK, Zamani Y, Zamanian A (2010) J Nat Gas Chem 19:193
16. Ojeda M, Nabar R, Nilekar AU, Ishikawa A, Mavrikakis M, Iglesia E (2010) J Catal 272:287
17. Puskas I, Hurlbut RS (2003) Catal Today 84:99
18. Stenger HG Jr (1985) J Catal 92:426
19. Amenomiya Y, Pleizier G (1973) J Catal 28:442
20. Wan H, Wu B, Zhang C, Xiang H, Li Y (2008) J Mol Catal A Chem 283:33
21. Zhang C, Zhao G, Liu K, Yang Y, Xiang H, Li Y (2010) J Mol Catal A Chem 328:35
22. Dry ME, Shingles T, Boshoff LJ, Oosthuizen GJ (1969) J Catal 15:190